Chapter IV

γ-irradiation induced PL quenching in Eu^{3+}:$GdVO_4$ nanosystems and related phosphorescence decay dynamic

It is well known that $REVO_4$ doped with luminescent Ln^{3+} ions play an important role as promising light-emitting materials **[1]**. Properties such as moderate cut-off phonon energy, relatively higher-luminescence quantum efficiencies and inherent stability are common in rare earth orthovanadates **[2-7]**. As a host matrix, tetragonal zircon-type gadolinium orthovanadate ($GdVO_4$) for RE activators was first studied by Zaguniennyi *et al.* in 1992 and shown to have more desirable as well as superior properties than YVO_4, such as higher thermal conductivity, stronger emission as well as absorption cross section **[8]**. In general, the direct excitation of Ln^{3+} ions are inefficient, owing to forbidden nature of 4*f*-4*f* transitions. However, it is the forbidden 4*f*–4*f* electronic transitions which offer sharp emission bands in the UV–vis range upon UV excitation **[9]**. Furthermore, Gd^{3+} ($^4f_7$, ^8S) based host matrices are significant phosphors due to relatively higher energy of the lowest excited state in connection with stability of a half-filled of the ground state of Gd **[1, 10]**. Phenomenon such as energy transfer (ET) and charge transfer (CT) thus play an important role in enhancing the luminescence efficiency **[1].** Furthermore, the properties of $REVO_4$ can be tweaked as per requirement upon introducing dopants into the host material turning them into exceptionally useful matrix materials **[6].** Among the different compounds, $GdVO_4$ are of special interest from the optical point of view as the excitation of the doped Ln^{3+} is mediated through an energy transfer from the vanadate anion thereby results in a higher luminescence **[11].** The need for shaping an effectual visible laser sources has driven researchers over the past few decades to draw their attention towards investigation of Ln^{3+} ions in various host matrices **[12]**. In particular, Eu^{3+} as a dopant in $GdVO_4$ has proven to be a highly efficient and intense red light-emitting phosphorescent material owing to strong absorption of UV radiation by the VO_3^{4-} groups and efficient energy transfer from host to dopant Eu^{3+} ions allowing it to be purposeful in many devices **[1, 6, 10, 13-15].** Eu^{3+} also exhibits well recognized pure red light-emitting center following highly intense $^5D_0 \rightarrow {}^7F_2$ electronic transition **[12].** Gd^{3+} has seven unpaired electrons which makes it suitable for magnetic resonance imaging, while the *D-F* transitions in Eu^{3+} allow it to perform

extremely well as red phosphors **[1, 3].** The combination of both lanthanide ions has been the basis for the development and characterization of most bifunctional contrast agents **[3, 16, 17].**

Various reports can be found in literature that deal with studies determining the optimum doping level for best PL emission profile. Nunez *et. al.* reported that 10 mol% Eu^{3+} dopant displayed the highest emission intensity in Eu^{3+} doped $GdVO_4$ nanocrystal (doping level from 2-15%). Moreover, while most phosphors display fluorescence quenching with increasing temperature, Eu^{3+}:$GdVO_4$ have applications in high temperature environments for their remarkable performance **[18]**. In the past few decades, usage of radiation such as influence of high energy photons (gamma or X-rays) have gained manifold applications, with continuous rise in interest in various fields *viz.* nanophotonics, agriculture and nuclear engineering, , space technology, clinical usage etc. **[19, 20].** It is worth mentioning that γ -rays are used in radiation radiography and medical equipment's sterilization in clinical research domain, while in agriculture, radiation treatment are largely utilized for food items to extend their shelf-life by destroying harmful pathogens without affecting the nutrition chains of the food items **[21].**

A radiation energy higher than the band gap of the material, has the potential to ionize the electrons from their valence band and thereby are free resulting in generation of positive holes captured by the already present intrinsic defects. It is noteworthy that to the best of our knowledge the interaction of γ rays with Gd based orthovandates doped with Ln^{3+} ions is scarcely found in literature. In this Chapter, we report a thorough investigation on Eu^{3+} doped $GdVO_4$ nanosystem to determine optical emission response and the critical concentration necessary for the luminescence quenching behaviour. The effects of radiation in the luminescence profile and the lifetime of tranititons involved are discussed in detail.

4.1. Excitation spectra

The excitation spectrum as shown in **FIGURE 4. 1 (a, b**) for the different samples was recorded targeting emission wavelength of 615 nm. The observed excitation spectrum is characterized by two major excitation bands corresponding to Eu^{3+}–O^{2-} and V^{5+}–O^{2-} charge transfers [3]. The asymmetric excitation band profile suggests overlap of additional excitation components on the higher energy side of the excitation band [22]. To reveal more information as regards the overlapping bands, the entire spectrum was subjected to deconvolution. The bands ranging in between ~220–270 nm are in general ascribed to the transitions toward the charge transfer state (CTS) due to Eu^{3+}– O^{2-} interactions [10]. However, the band observed at ~254 nm can be attributed to a charge transfer (CT) process from oxygen ligands to the central vanadium ions inside the $[VO_4]^{3-}$ groups [23, 24]. The broad band at ~254 nm has also been assigned to the host ion based ^8S–^6D transition [18].

Characteristic Eu^{3+} excitation bands usually appear beyond 350 nm, including the observed $^7F_0$-$^5D_3$ transition [18]. It is noteworthy that band corresponding to the intra-f transitions within the $^4f_6$ configuration of the Eu^{3+} ions, typically ascribed to $^7F_0 \rightarrow {}^5L_6$ and $^7F_{0,1} \rightarrow {}^5D_2$ of Eu^{3+} ion were observed at ~ 395 nm and 459 nm respectively [25-27]. The ~395 nm band is the characteristic band for Eu^{3+}, however its intensity was determined to be comparatively weaker than that of the ET transitions from $[VO_4]^{3-}$ -Eu^{3+}. This implies that ET transitions from $[VO_4]^{3-}$ to Eu^{3+} are more efficient excitation pathways for the characteristic red emission of Eu^{3+} [24]. The possibility of efficient energy transfer between $[VO_4]^{3-}$ to Eu^{3+} ions has been reported earlier [16, 18]. It is known that under UV excitation, the energy migrates easily through $[VO_4]^{3-}$ group and then transfers to the dopant RE ions activators leading to the characteristic *f-f* transitions [27]. In such case, host Gd^{3+} ions act as effective sensitizing ions as the Gd^{3+} $^4f_7$, ^8S has its lowest excited state levels at relatively higher energy values as a consequence of stability of the half-filled shell ground state [4, 27].

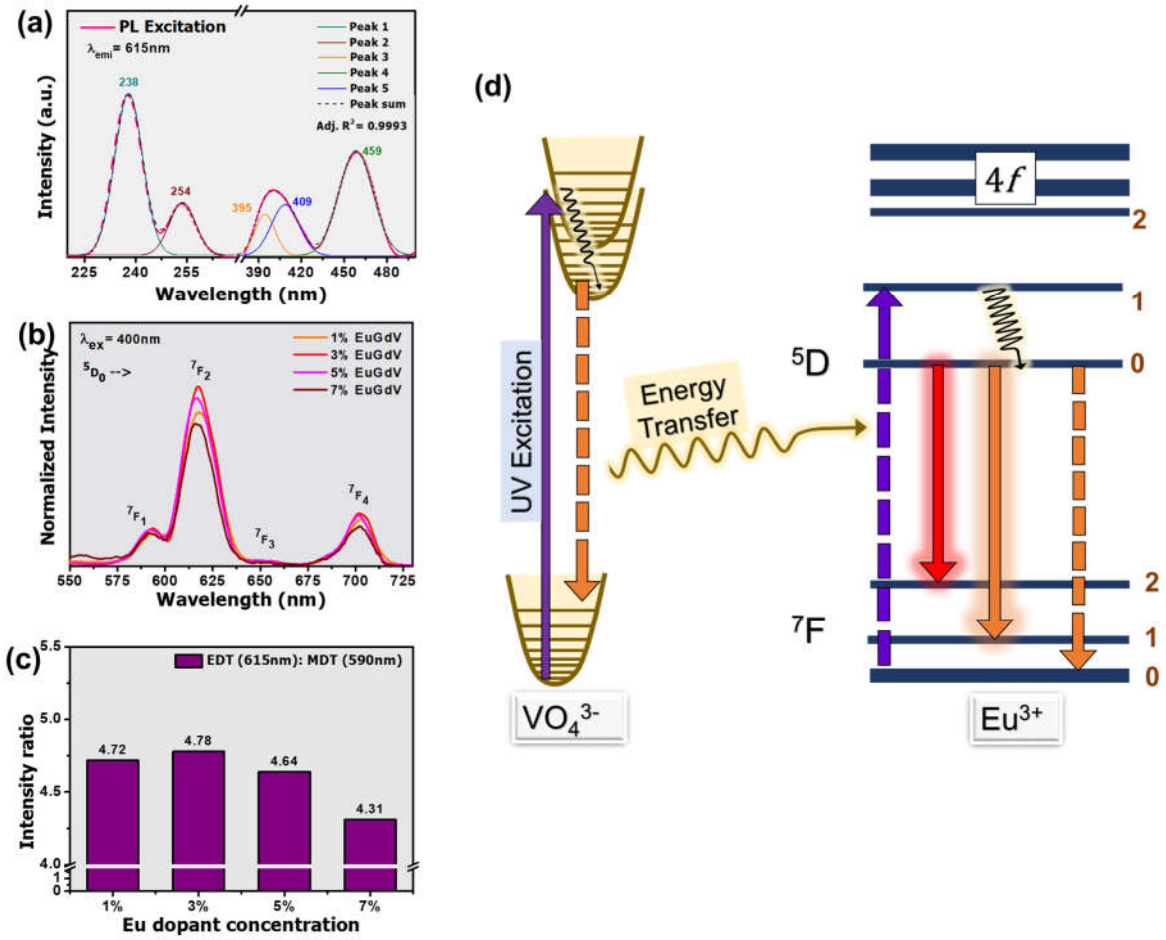

Figure 4.1. Photoluminescence (a) excitation spectra and (b) emission spectra of nanophosphors. (c) Red- orange emission intensity ratio for samples doped with different Eu^{3+} concentration. (d) Model for emission processes involved in Eu^{3+}:$GdVO_4$ depicting efficient excitation route.

4.2. PL Emission profile

It is widely known that under UV excitation, Eu^{3+} doped $GdVO_4$ nanoparticles display intense red luminescence due to transitions within f- shell of the Eu^{3+} ions [28]. The normalized emission profiles of the nanosystem excited at 400 nm can be observed in **Figure 4.1(c).** Important transitions observed are $^5D_0 \rightarrow {}^7F_{1,2,3}$ of which the most intense peak was found to be the $^5D_0 \rightarrow {}^7F_2$ transition. The mechanism of energy transfer between the host and dopant involves four steps, (i) host sensitizer (with creation of a Frenkel exciton), (ii) migration of exciton within the $[VO_4]^{3-}$ sublattice, (iii) energy transfer to activator ions, and (iv) PL emission [29]. It is

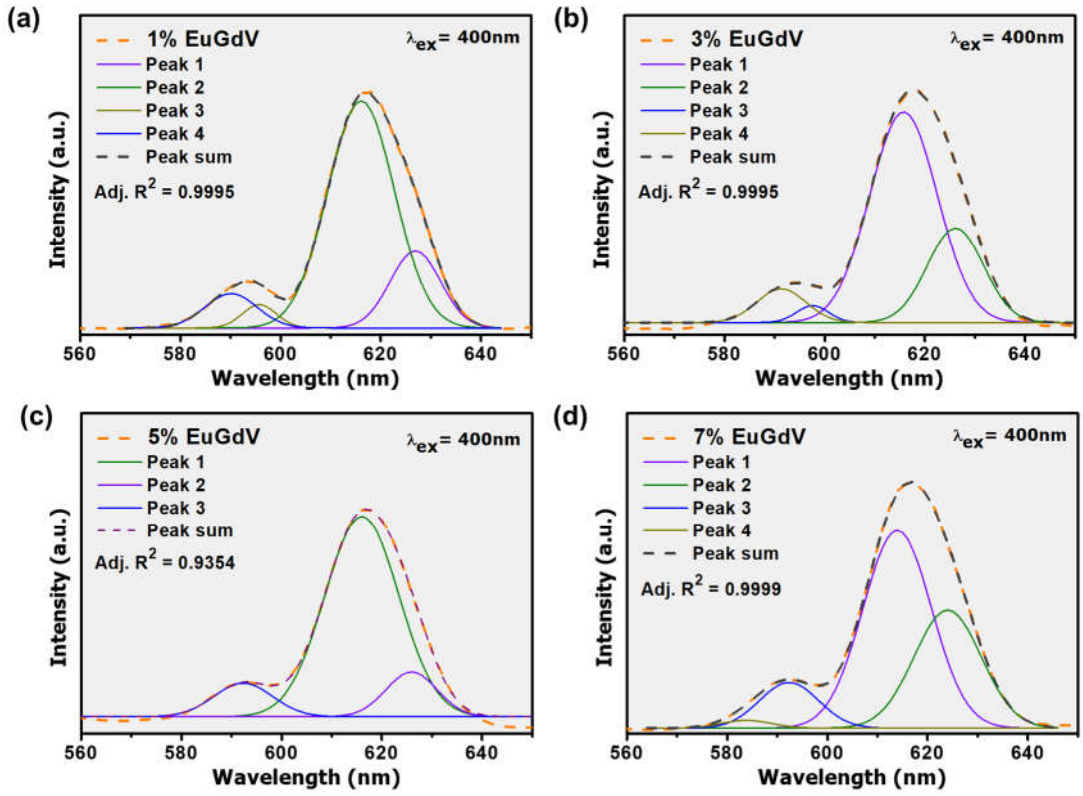

Figure 4.2. Deconvoluted emission profiles of (a) 1% EuGdV (b) 3% EuGdV (c) 5% EuGdV and (d) 7% EuGdV, excited at 400nm

important to note that migration of Frenkel excitons can lead to lattice distortions as for exciton-lattice interactions, the excitation is coupled to the lattice creating lattice distortions which travels adiabatically with the electronic excitation [30].

Among all the emission spectral lines observed, $^5D_0$-$^7F_2$ (~615 nm) and $^5D_0$-$^7F_3$ (~650 nm) transitions originate from Eu^{3+} located at the C_2 sites by the electric dipole transition and $^5D_0 \rightarrow {}^7F_1$ by magnetic dipole transition positioned at both S_6 and C_2 sites [29, 31]. MDT in RE ions are allowed transitions while the electric dipole transitions are forbidden. The local symmetry around the dopant activator ions without an inversion centre, are responsible for lifting parity forbiddance leading them to be partially allowed [32]. MDT is generally observed only between states of the same parity and thus are not sensitive to the host matrix as EDT [33]. The most intense MDT is observed at ~590 nm for $^5D_0 \rightarrow {}^7F_1$ while the most prominent peak in the spectra is the host-dependent EDT is, otherwise termed hypersensitive $^5D_0 \rightarrow {}^7F_2$ transition positioned at 615 nm. Interestingly, the

$^5D_0$-$^7F_0$ transition usually observed at ~580 nm was not observed in our case. The transition is strongly forbidden in the D_{2d} symmetry [29]. It is well known that alternative edge-sharing VO_4 tetrahedra and GdO bisdisphenoids extending parallel to c-axis which are laterally joined by edge-sharing bisdisphenoids are realised in crystalline tetragonal $GdVO_4$. Also, GdO_8 dodecahedra have two sets of four equal Gd–O bond lengths: short and long involving the point symmetry $\boldsymbol{D_{2d}}$ of $Gd^{3+,}$ with no inversion centre. It is argued that the emission peak due to hypersensitive $^5D_0 \rightarrow {}^7F_2$ transition is dominant as for the Eu^{3+} substitutes the Gd^{3+} lattice of D_{2d} site symmetry which is highly asymmetric [25]. This explains the dominant nature of the $^5D_0 \rightarrow {}^7F_2$ in the emission spectra. Additionally, no emission peaks from the $[VO_4]^{3-}$ group were detected which implies effectual $[VO_4]^{3-}$ to Eu^{3+} ET [15, 34].

As observed from **FIGURE 4.1(c),** upon varying the dopant concentration, the intensity for the $^5D_0 \rightarrow {}^7F_2$ transition was found to increase and find a maximum value at 3 mol% dopant concentration, beyond which, the intensity decreased. Such variation was speculated as a consequence of inhomogeneous distribution of the dopant ions in the host lattice and thereby the local symmetry is compromised. Eventually the hypersensitive EDT is effected while the MDT remains almost unaffected. The observation of drop in the intensity around 5mol % Eu concentration can be assigned to concentration quenching effect [15]. In general, increment in the concentration of Eu^{3+} ions leads to decrement in the inter-ionic distance between dopants, thereby promoting Eu–Eu interactions which ultimately results in cross relaxation processes [3, 11]. To be mentioned, multiphonon relaxation, concentration quenching and the cross-relaxation between neighbouring Eu^{3+} ions, quench the $^5D_0 \rightarrow {}^7F_{1,2,3,4}$ transitions substantially [35]. In order to determine if any splitting has occurred, we de-convoluted the spectra as shown in Figure 4.2. We observed prominent overlap of peaks at the red regime- ~598 nm, 615 nm, and 625 nm. It is also to be noted that the PL emission intensity ratio of EDT (615 nm) to MDT (590 nm) i.e. (Red to Orange ratio), enables us to assess important information about the symmetry as

well as covalent nature at the site occupied by Eu^{3+} ions in the host matrix. [33, 35, 36]. A greater value of the ratio or inequality in the intensities of the two transitions implies larger asymmetry and henceforth the ratio can also have termed as the asymmetric ratio [29, 32]. In fact, higher EDT:MDT intensity ratio implies that the local symmetry around dopant ions is closer to an inversion centre [33]. The effect of the dopant concentration in altering the EDT:MDT intensity ratio can be assessed using **FIGURE 4.1(c).** The EDT:MDT intensity ratio was determined to be greater than 1 in all the cases which implies that dopant ions are situated at the higher asymmetry sites where the local site symmetry is deviated from inverse centre **[35].** Also, upon increasing the dopant concentration from 1 to 3mol% led to subtle rise in the ratio. Distortion introduced in the lattices and the oxygen deficiencies in the nanosized systems may increase the degree of disorder and lower the local symmetry of Eu^{3+} ions, and as a consequence, the probability for the $^5D_0 \rightarrow {}^7F_2$ transition to occur is increased but then again dropped beyond 5% [32]. As discussed earlier, the observation is attributed to quenching effects and processes involved thereof including non-radiative energy dissipation between neighbouring Eu^{3+} ions. Increment in the dopant concentration implies closer site allocation and consequently the probability of inter ionic non-radiative energy transfer increases. This leads to rise in metastable excited states within the host matrix and consequently nonradiative de-excitation via quenching centers or traps tends to increase too **[22, 32]**. The entire process viz. UV excitation of host sensitizer and energy transfer to dopant activator followed by radiative and non-radiative events is illustrated in **FIGURE 1(d).**

Knowing that the inter ionic separation plays an important role in determining the quenching effect, the critical distance, R_c for the critical concentration, X_c= 3 mol% was determined using Blasse's energy transfer equation (Eq.5) and was found to be ~1.86 Å [15, 37-39],

$$R_C = \left(\frac{3V}{4\pi N X_c}\right)^{\frac{1}{3}}, \qquad (5)$$

where, '*N*' is number of cations per unit cell '4' for GdV and '*V*' is the unit cell volume determined using '*Powder cell for Windows®*' to be 325.3 $Å^3$.

It is generally considered that the degree of disorder in the nanoparticles is relatively high, and so a lower crystal field symmetry might be induced in such materials [32]. RE based nanosystems display characteristic stark-crystal field splitting in the emission profile of the dopant ions [31, 35]. In nanostructures, the deficiency of the traps due to the limited primitive cells per particle results in the fact that the traps distribute randomly with a considerable fluctuation in distribution between particles [32]. In such a case, the number of traps vary from particle to particle. Increasing the concentration of luminescent centers, quenching occurs first in particles containing more traps, while those particles with few or no traps quench only at high concentration or do not quench at all [32]. Furthermore, asymmetrical $^5D_0 \rightarrow {}^7F_2$ emission lines also imply presence of distortions in the system around activator ions [29]. Defect formation can also occur in a RE vanadate host system as a consequence of difference in hydroxylation state between the host and dopant Eu^{3+} ions prior to the formation of the vanadate lattice [29] .

4.3 Effect of γ-irradiation on emission spectra

By and large, γ irradiation are responsible for atomic knockouts, ionizations and modifications in electron densities of the hosts in a dose dependent manner [40]. Reports available in the literature also suggest that the emission intensity decrease considerably for γ-irradiation beyond ~2 kGy doses [20, 40-42]. Such γ-irradiation dose dependent luminescence quenching can be attributed to partial transfer of excitation and/or emission energy of the activator ions towards the defect centers/trapped charges (tracks) induced upon irradiation [20]. It is known that the defects in the phosphors in general favour non-radiative process as a consequence of which the emission intensity would decline [43]. Possibility of partial excitation/emission energy migration to defect/trap centres created by

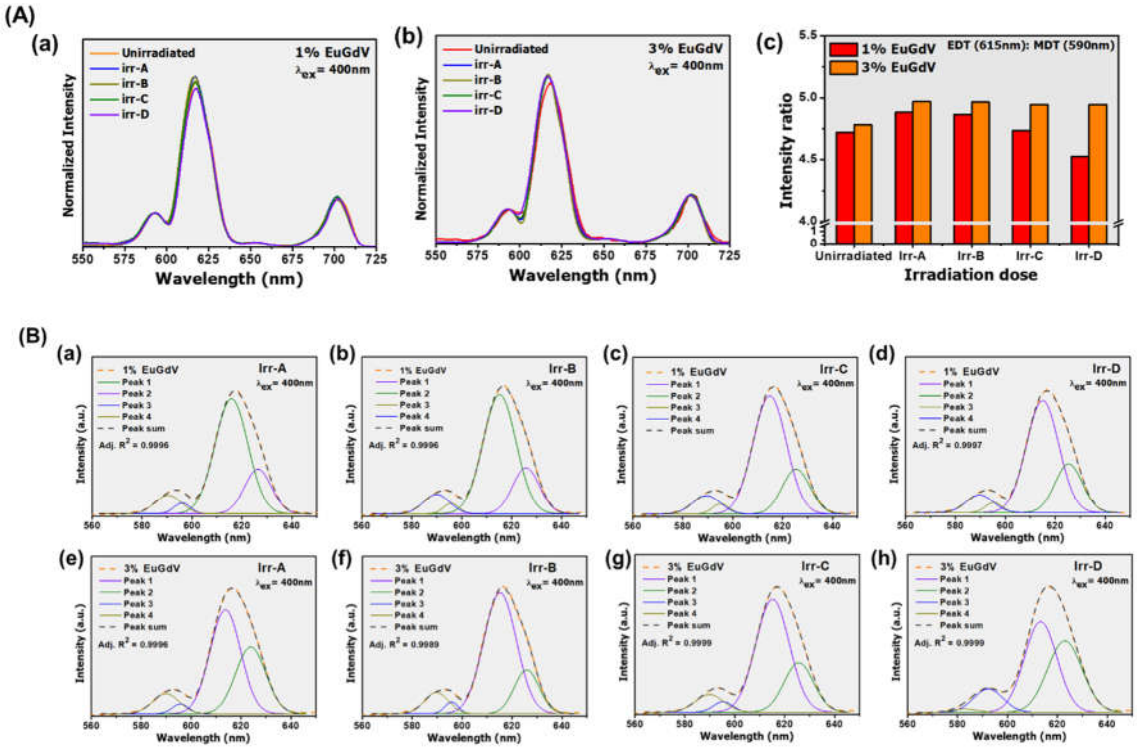

Figure 4.3. Normalized PL emission profiles of unirradiated and γ-irradiated (a) 1% EuGdV and (b) 3% EuGdV with the R/O intensity ratios displayed in (c). (B) The deconvolved PL spectra for 1% EuGdV is shown in (a-d) and for 3% EuGdV in (e-h).

radiation cannot be disregarded which might play a role in luminescence quenching of Eu^{3+} emission profile [20, 42]. Moreover, γ-irradiation can typically absorb light via creation F centres [42].

Similar luminescence quenching threshold of g-irradiation dose (~1kGy) has earlier been reported in literature **[44].** Interestingly, γ- irradiation induced quenching is more prominent in 1% EuGdV system as compared to 3% EuGdV system. This observation can be described considering the difference in dopant concentration and thereby the number of luminescent centres available in the matrix. Earlier, decrement in luminescence of Eu^{3+} doped ABO_4 nanophosphor upon γ-irradiation was explained using 'track interaction model' (TIM) [45]. TIM suggests that for a nanocrystalline phosphor, the extents of the tracks formed due to ionizing radiation will be of nanoparticle dimension and hence number of trapping centers (TC) created at lower doses would be reasonably less **[46].**

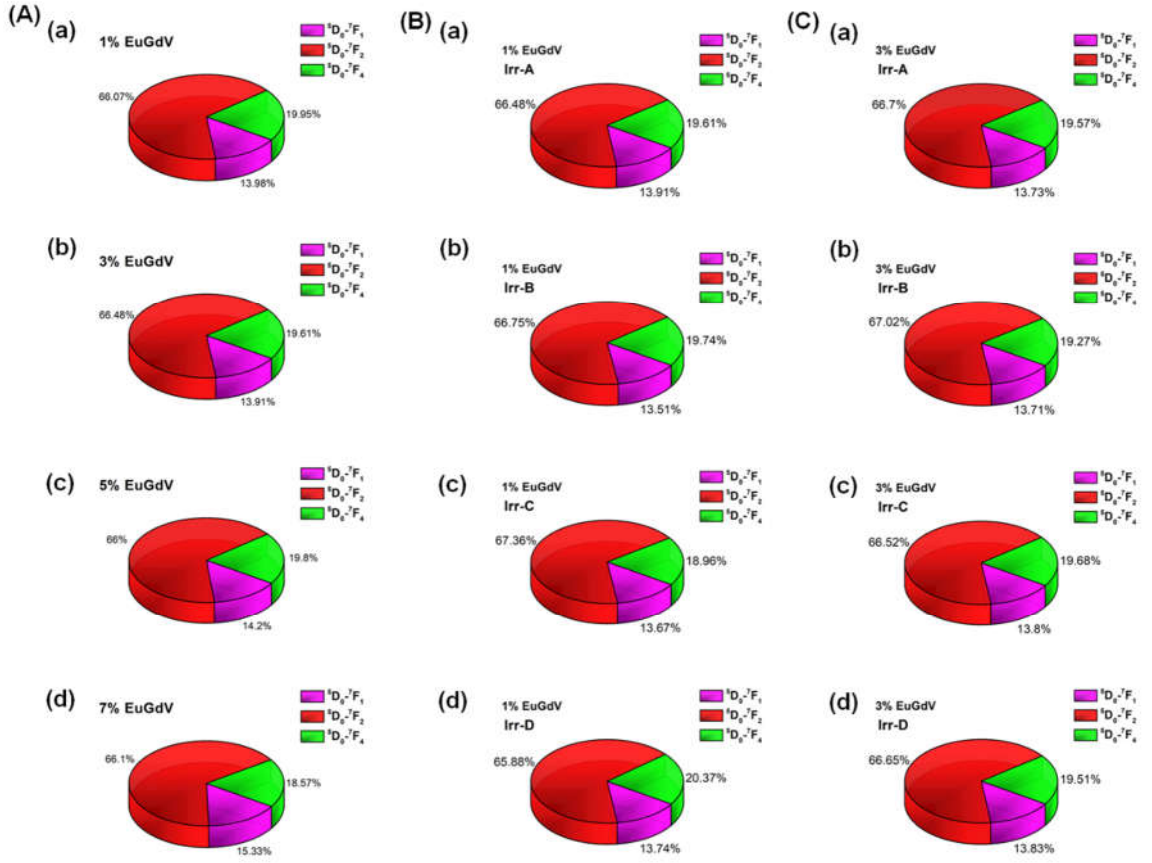

FIGURE 4.4. Pie chart illustrating proportion of the emission intensities in (A) various concentrations of (a) 1% EuGdV (b) 3% EuGdV (c) 5% EuGdV and (d) 7% EuGdV; while (B) and (C) demonstrate the same for 1% EuGdV and 3% EuGdV upon g-irradiation of various doses (a) Irr-A (b) Irr-B (c) Irr-C and (d) Irr-D respectively.

However, for higher radiation dose, overlapping and accumulation of such tracks can lead to saturation as well as decrement in the luminescence intensity **[47].** In addition, higher number of activator ions i.e. dopant Eu^{3+} ions imply greater radiative events to occur and thereby diminishes the impact of defect mediated non-radiative transitions responsible for g-irradiation induced quenching effect in the spectral profile. Such insensitive nature towards g-irradiation of the transitions from $^5D_0$ level has also been ascribed to the characteristic shielding effect of 4*f* orbital electrons by the outer 5*s* and 5*p* orbitals for RE ions, in this case Eu^{3+} ions **[43].** We conclude that irradiation doses beyond a specific value does not influence the luminescence wavelength distribution of the Eu^{3+} doped at

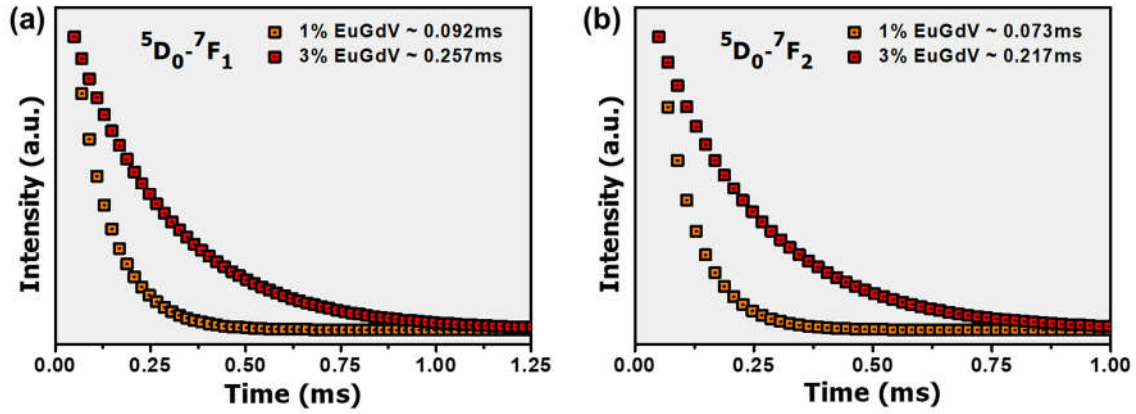

Figure 4.5. TRPL lifetime decay dynamics of (a) $^5D_0$-$^7F_1$ and (b) $^5D_0$-$^7F_2$ in 1% EuGdV and 3% EuGdV

critical concentration. A Pie-diagram demonstrating the proportion of the emission intensities has been prepared to have a brief overview of the effect of dopant concentration and γ-irradiation dose on EDT and MDT in the as prepared samples as shown in **FIGURE 4.4.**

4.4 Decay analysis

In order to determine the effect of irradiation in the metastable states of activator ions, photoluminescence decay curves were analysed. In **FIGURE 4.5**, γ-dose dependent lifetime decay curves are displayed for 1% EuGdV and 3% EuGdV, which were found to be best fit in accordance with single exponential equation [48]. We found that upon increasing the dopant concentration, the average lifetime has increased. Dopant inclusions introduce defects in the crystal which can thereby result in a longer recombination route and hence an increase in lifetime. Moreover, other important factors which can result in a longer radiative lifetime of $^5D_0$ transitions for Eu^{3+} in Gd based nanocrystals are (i) the non-solid medium surrounding the nanoparticles changing the effective refraction index (ii) increased lattice constant upon dopant inclusion [49, 50].

Interestingly, upon irradiation with highly energetic γ-rays, we recorded decrement in the average lifetime calculated, as shown in **FIGURE 4.6** and **FIGURE 4.7** [19]. The lifetime values of 3% EuGdV for the important transitions

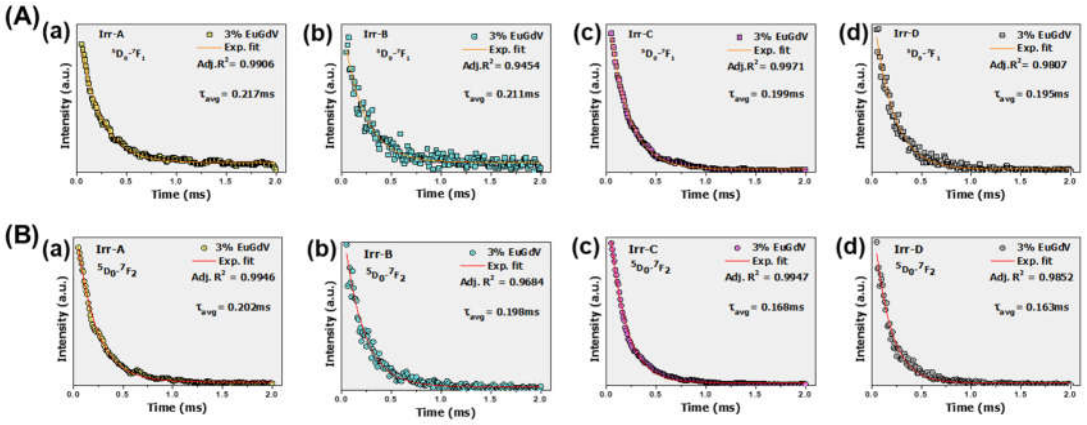

Figure 4.6. TRPL lifetime decay dynamics of (A) $^5D_0$-$^7F_1$ and (B) $^5D_0$-$^7F_2$ emission in 3% EuGdV irradiated with (a) Irr-A (b) Irr-B (c) Irr-C and (d) Irr-D respectively.

($^5D_0 \rightarrow {}^7F_{1,2}$) were determined to be longest for the unirradiated sample. with decreasing trend was observed with irradiation doses (**FIGURE 4.6**). For the MDT, $^5D_0 \rightarrow {}^7F_1$ positioned at ~590 nm, lifetime dropped from ~0.26 ms for unirradiated sample to ~0.217 ms for Irr-A and further decreased in a linear trend to ~0.19 ms upon highest γ-dose considered (Irr-D). Similar observation could be made in case of the most intense transition $^5D_0$-$^7F_2$ (~615nm) wherein the decay lifetime decreased from 0.22ms for unirradiated sample to 0.16ms for Irr-A following a linear trend with a negative slope as the γ-dose was raised. Very limited reports are available in the literature that discuss effect of γ-irradiation in the lifetime decay profiles of RE doped $GdVO_4$ nanosystems.

Very limited reports are available in the literature that discusses the effect of γ–irradiation. No change in lifetime of metastable states of Eu^{3+} after γ-irradiation was inferred as the probability of change in oxidation state of Eu^{3+} is negligible [20]. Viswanath *et al.* have reported decrement in the decay parameter of RE doped $GdVO_4$ upon γ-irradiation [42]. In another report, decrease in the lifetime with increase in γ-dose was ascribed to defect mediated quenching of the excited state [40]. A decreasing trend of lifetime can also be ascribed to an increase in the spontaneous emission transition probability as a consequence of compromise of local symmetry of Eu^{3+} ions due to defect manifestation **[51].** The

observed lifetime quenching can be attributed to the ET processes owing to the

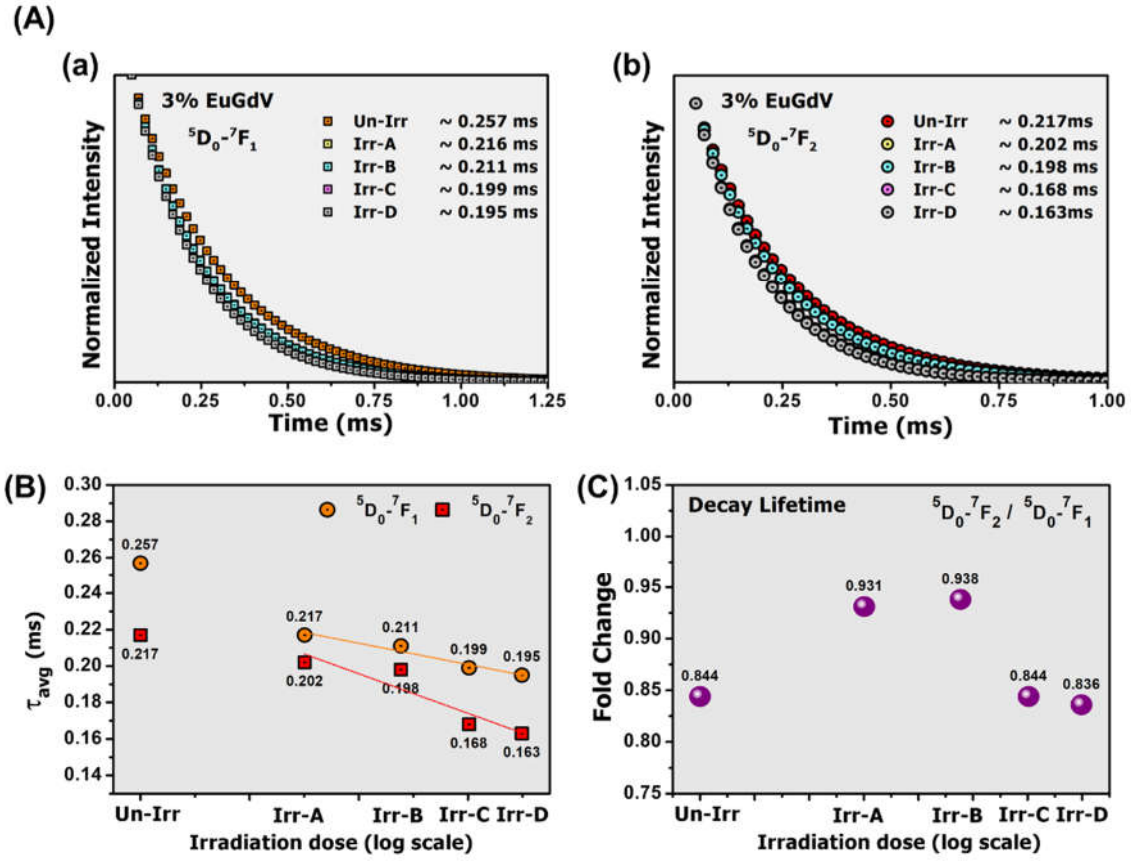

Figure 4.7. (A) Exponential fit profiles of TRPL lifetime decay dynamics in 3% EuGdV for (a) $^5D_0$-$^7F_1$ and (b) $^5D_0$-$^7F_2$ emission. The linear fit profile for average lifetime determined upon irradiation with various doses is displayed in (B) and (C) shows the fold change in the major emission lines upon irradiation.

cross-relaxation and/or non-radiative relaxation channels involved in the phosphor **[40, 42].** It is known that the distortions in local environment of Eu^{3+} lowers the probability of a radiative transition **[52].** Thus, greater γ-doses imply greater probability of non- radiative de-excitation via distortions induced in the lattice sites of the dopant Eu^{3+} ions, which are regarded as a major contributor to decrement in average luminescence decay lifetime, as observed **[3].**

As discussed earlier, the excitation pathway involves Frenkel exciton migration. The Frenkel exciton migration occurs via two routes, direct diffusion model and/or nearest neighbor hopping random walk model [53]. An exciton can

be treated as a quasi-particle which can transfer energy acting as excited sensitizer to the activators acting as excitonic traps to absorb the energy completely. In hopping model, an incident photon excites the host to be eventually transfered to nearest neighbours. If nearest neighbour is a host site, either hopping of the exciton continues further or photoemission occurs. Alternatively, if the newly stepped on site is a trap/dopant, the walk stops and emission of a trap fluorescence photon occurs with a constant energy transfer rate given by the following equation: **[53]**

$$k = 4\pi DRN_t \quad (6)$$

where, D is the diffusion coefficient of Frenkel excitons, *R* is the radius of activator Eu^{3+} (exciton traps) and N_t is the trap concentration. Clearly, for Frenkel exciton diffusion the energy transfer rate is independent of time, and is proportional to dopant concentration. Again, in terms of the lifetime of the Frenkel excitons, the rate constant is given by **[53]:**

$$k = \frac{1}{\tau_s} - \frac{1}{\tau_s^0} \quad (7)$$

where t_s, t_s^0 are the lifetimes of sensitizer in presence and absence of the activator. Hence, exciton quenching can lead to reduction of PL decay parameters [54]. In such consideration, trapped excitons are usually quenching sites since the defects do not show phosphorescent behaviour. Furthermore, non-radiative exciton dissociation into free electrons and holes can take place and PL emission quenching occurs subsequently [54]. Considering a phosphor, triplet excitons are expected to have longer diffusion length than singlets due to their much longer lifetime (in the order of a few ~ms) considering exchange interactions involved. However, the relevant Frenkel exciton displays a lifetime in the order of ps, or ns [54, 55]. Since γ-irradiation can lead to generation of Frenkel defects, the contribution of Frenkel excitons quenching and consequently decrement in lifetime of the prominent $^5D \rightarrow {}^7F$ transitions cannot be ignored and needs detailed evaluation to understand the underlying mechanisms involved.

4.5. Conclusion

The luminescence profiling of the prepared samples were undertaken and the photoluminescence excitation spectra depicted two major excitation bands assigned to Eu^{3+}–O^{2-} and V^{5+}–O^{2-} charge transfer processes. The emission profiles suggest that Eu^{3+} substitutes highly asymmetric $\mathbf{D}_{2d}$ site of the Gd^{3+} lattice explaining the dominant nature of the ${}^5D_0 \rightarrow {}^7F_2$ and no show up of the ${}^5D_0 \rightarrow {}^7F_0$. Whereas, no emission peaks from the $[VO_4]^{3-}$ group were detected it is concluded that ET transitions from $[VO_4]^{3-}$ to Eu^{3+} is more efficient excitation pathway for the characteristic red emission of Eu^{3+}. Interestingly, luminescence quenching effects were observed beyond a critical dopant concentration of 3 mol% offering maximal PL intensity for which, inter-activator distance was calculated to be ~1.86 Å. It is to be highlighted that in addition to the dopant concentration dependent quenching, we also observed γ-irradiation dose dependent luminescence quenching. Such an important observation is attributed to partial transfer of excitation/emission energy of activator ions towards the defect centers/trapped charges introduced upon irradiation. Furthermore, lifetime quenching was also observed ascribed to the ET processes owing to the cross-relaxation and/or non-radiative relaxation channels involved in the phosphor. The determined parameters for 3% EuGdV samples are compared for better understanding with that for 3% EuGNP and is presented in Table 1, Appendix-I. The observations made needs further detailed investigation as to establish proper energy transfer mechanisms involved in the RE based nanophosphors.

Bibliography:

[1] Szczeszak, A., Ekner-Grzyb, A., Runowski, M., Mrówczyńska, L., Grzyb, T., and Lis, S., Synthesis, photophysical analysis, and in vitro cytotoxicity assessment of the multifunctional (magnetic and luminescent) core@ shell nanomaterial based on lanthanide-doped orthovanadates. *Journal of Nanoparticle Research*, 17(3):1-11, 2015.

[2] Gavrilović, T.V., Jovanović, D.J., Smits, K., and Dramićanin, M.D., Multicolor upconversion luminescence of $GdVO_4:Ln^{3+}/Yb^{3+}$ (Ln^{3+}= Ho^{3+}, Er^{3+}, Tm^{3+}, $Ho^{3+}/Er^{3+}/Tm^{3+}$) nanorods. *Dyes and pigments*, 126:1-7, 2016.

[3] Toro-González, M., Copping, R., Mirzadeh, S., and Rojas, J.V., Multifunctional $GdVO_4$: Eu core–shell nanoparticles containing 225 Ac for targeted alpha therapy and molecular imaging. *Journal of Materials Chemistry B*, 6(47):7985-7997, 2018.

[4] Singh, N.S., Ningthoujam, R., Phaomei, G., Singh, S.D., Vinu, A., and Vatsa, R., Re-dispersion and film formation of $GdVO_4$: Ln^{3+} (Ln^{3+}= Dy^{3+}, Eu^{3+}, Sm^{3+}, Tm^{3+}) nanoparticles: particle size and luminescence studies. *Dalton Transactions*, 41(15):4404-4412, 2012.

[5] Brites, C.D., Lima, P.P., Silva, N.J., Millan, A., Amaral, V.S., Palacio, F., and Carlos, L.D., Lanthanide-based luminescent molecular thermometers. *New Journal of Chemistry*, 35(6):1177-1183, 2011.

[6] Nikolić, M.G., Jovanović, D.J., and Dramićanin, M.D., Temperature dependence of emission and lifetime in Eu^{3+} and Dy^{3+}-doped $GdVO_4$. *Applied Optics*, 52(8):1716-1724, 2013.

[7] Ryba-Romanowski, W., Lisiecki, R., Jelinková, H., and Šulc, J., Thulium-doped vanadate crystals: Growth, spectroscopy and laser performance. *Progress in Quantum Electronics*, 35(5):109-157, 2011.

[8] Ostroumov, V., Shcherbakov, I., Zagumennyi, A., Huber, G., Jensen, T., and Meyn, J. Nd:$GdVO_4$ Crystal—A new material for diode-pumped solid-state lasers. in Advanced Solid State Lasers. NL1: *Optical Society of America*, 1993.

[9] Ramesh, P., Hegde, V., Keshavamurthy, K., Pramod, A., Jagannath, G., Aloraini, D.A., Almuqrin, A.H., Sayyed, M., Harisha, K., and Khan, S., Influence of gamma irradiation on photoluminescence and nonlinear optical properties of Eu^{3+} activated heavy metal borate glasses. *Optical Materials*, 116:111102, 2021.

[10] Wu, J. and Yan, B., Photoluminescence intensity of $Y_xGd_{1-x}VO_4$:Eu3+ dependence on hydrothermal synthesis time and variable ratio of Y/Gd. *Journal of Alloys and Compounds*, 455(1-2):485-488, 2008.

[11] Nuñez, N.O., Rivera, S., Alcantara, D., Jesus, M., García-Sevillano, J., and Ocaña, M., Surface modified Eu:$GdVO_4$ nanocrystals for optical and MRI imaging. *Dalton Transactions*, 42(30):10725-10734, 2013.

[12] Manasa, P. and Jayasankar, C., Luminescence and phonon side band analysis of Eu3+-doped lead fluorosilicate glasses. *Optical Materials*, 62:139-145, 2016.

[13] Morris, P., Lüthy, W., Weber, H., Zavartsev, Y.D., Studenikin, P., Shcherbakov, I., and Zagumenyi, A., Laser operation and spectroscopy of Tm: Ho:$GdVO_4$. *Optics communications*, 111(5-6):493-496, 1994.

[14] Wang, F., Xue, X., and Liu, X., Multicolor tuning of (Ln, P)-Doped YVO_4 nanoparticles by single-wavelength excitation. *Angewandte Chemie*, 120(5):920-923, 2008.

[15] Li, X., Yu, M., Hou, Z., Li, G., Wang, W., Cheng, Z., and Lin, J., One-dimensional $GdVO_4:Ln^{3+}$ (Ln= Eu, Dy, Sm) nanofibers: electrospinning preparation and luminescence properties. *Journal of Solid State Chemistry*, 184(1):141-148, 2011.

[16] Abdesselem, M., Schoeffel, M., Maurin, I., Ramodiharilafy, R., Autret, G., Clément, O., Tharaux, P.-L., Boilot, J.-P., Gacoin, T., and Bouzigues, C., Multifunctional rare-earth vanadate nanoparticles: luminescent labels, oxidant sensors, and MRI contrast agents. *ACS Nano*, 8(11):11126-11137, 2014.

[17] Kim, T., Lee, N., Park, Y.I., Kim, J., Kim, J., Lee, E.Y., Yi, M., Kim, B.-G., Hyeon, T., and Yu, T., Mesoporous silica-coated luminescent Eu^{3+} doped $GdVO_4$ nanoparticles for multimodal imaging and drug delivery. *RSC Advances*, 4(86):45687-45695, 2014.

[18] Jin, D., Yang, H., Ding, G., Yu, X., Wang, L., and Zheng, Y., Hydrothermal synthesis and photoluminescence behavior of Eu-doped $GdVO_4$. *Inorganic Materials*, 44(10):1121-1124, 2008.

[19] Sharma, G., Bagga, R., Cemmi, A., Falconieri, M., and Baccaro, S., Spectroscopic investigations on γ-irradiated Eu^{3+} and Dy^{3+} doped oxyfluoride glasses. *Radiation Physics and Chemistry*, 108:48-53, 2015.

[20] Hegde, V., Chauhan, N., Kumar, V., Viswanath, C.D., Mahato, K., and Kamath, S.D., Effects of high dose gamma irradiation on the optical properties of Eu^{3+} doped zinc sodium bismuth borate glasses for red LEDs. *Journal of Luminescence*, 207:288-300, 2019.

[21] Lakshminarayana, G., Baki, S., Kaky, K.M., Sayyed, M., Tekin, H., Lira, A., Kityk, I., and Mahdi, M., Investigation of structural, thermal properties and shielding parameters for multicomponent borate glasses for gamma and neutron radiation shielding applications. *Journal of Non-Crystalline Solids*, 471:222-237, 2017.

[22] Dhanaraj, J., Jagannathan, R., Kutty, T., and Lu, C.-H., Photoluminescence characteristics of $Y_2O_3:Eu^{3+}$ nanophosphors prepared using sol− gel thermolysis. *The Journal of Physical Chemistry B*, 105(45):11098-11105, 2001.

[23] Yang, L., Li, G., Zhao, M., Zheng, J., Guan, X., and Li, L., Morphology-controllable growth of $GdVO_4:Eu^{3+}$ nano/microstructures for an optimum red luminescence. *Nanotechnology*, 23(24):245602, 2012.

[24] Xu, W., Wang, Y., Bai, X., Dong, B., Liu, Q., Chen, J., and Song, H., Controllable synthesis and size-dependent luminescent properties of YVO_4: Eu^{3+} nanospheres and microspheres. *The Journal of Physical Chemistry C*, 114(33):14018-14024, 2010.

[25] Singh, N.S., Ningthoujam, R., Devi, L.R., Yaiphaba, N., Sudarsan, V., Singh, S.D., Vatsa, R., and Tewari, R., Luminescence study of Eu^{3+} doped $GdVO_4$

nanoparticles: Concentration, particle size, and core/shell effects. *Journal of Applied Physics*, 104(10):104307, 2008.

[26] Singh, L.R. and Ningthoujam, R., Critical view on energy transfer, site symmetry, improvement in luminescence of Eu^{3+}, Dy^{3+} doped YVO_4 by core-shell formation. *Journal of Applied Physics*, 107(10):104304, 2010.

[27] Singh, N.S., Ningthoujam, R., Yaiphaba, N., Singh, S.D., and Vatsa, R., Lifetime and quantum yield studies of Dy^{3+} doped $GdVO_4$ nanoparticles: concentration and annealing effect. *Journal of Applied Physics*, 105(6):064303, 2009.

[28] Riwotzki, K. and Haase, M., Colloidal YVO_4:Eu and $YP_{0.95}V_{0.05}O_4$:Eu nanoparticles: luminescence and energy transfer processes. *The Journal of Physical Chemistry B*, 105(51):12709-12713, 2001.

[29] Mialon, G., Turkcan, S., Alexandrou, A., Gacoin, T., and Boilot, J.-P., New insights into size effects in luminescent oxide nanocrystals. *The Journal of Physical Chemistry C*, 113(43):18699-18706, 2009.

[30] Zwemer, D., Energy transfer in anisotropic systems: A. Excitation migration in substitutionally disordered one-dimensional solids. B. The spectroscopy of molecules adsorbed on metal surfaces. 1978.

[31] Swapna, K., Mahamuda, S., Rao, A.S., Sasikala, T., Packiyaraj, P., Moorthy, L.R., and Prakash, G.V., Luminescence characterization of Eu^{3+} doped Zinc Alumino Bismuth Borate glasses for visible red emission applications. *Journal of Luminescence*, 156:80-86, 2014.

[32] Wei, Z., Sun, L., Liao, C., Yin, J., Jiang, X., Yan, C., and Lü, S., Size-dependent chromaticity in YBO_3:Eu nanocrystals: correlation with microstructure and site symmetry. *The Journal of Physical Chemistry B*, 106(41):10610-10617, 2002.

[33] Reisfeld*, R., Zigansky, E., and Gaft, M., Europium probe for estimation of site symmetry in glass films, glasses and crystals. *Molecular Physics*, 102(11-12):1319-1330, 2004.

[34] Gupta, B.K., Rathee, V., Narayanan, T.N., Thanikaivelan, P., Saha, A., Singh, S., Shanker, V., Marti, A.A., and Ajayan, P.M., Probing a Bifunctional Luminomagnetic Nanophosphor for Biological Applications: a Photoluminescence and Time-Resolved Spectroscopic Study. *Small*, 7(13):1767-1773, 2011.

[35] Reddy, A.A., Das, S., Ahmad, S., Babu, S.S., Ferreira, J.M., and Prakash, G.V., Influence of the annealing temperatures on the photoluminescence of $KCaBO_3:Eu^{3+}$ phosphor. *RSC Advances*, 2(23):8768-8776, 2012.

[36] Prakash, G.V. and Jagannathan, R., Fluorescence properties of Eu^{3+} doped lead bearing fluoro-chloro phosphate glasses. *Spectrochimica Acta Part A: Molecular and Biomolecular Spectroscopy*, 55(9):1799-1808, 1999.

[37] Blasse, G., Energy transfer in oxidic phosphors. *Philips Res. Rep*, 24(2):131, 1969.

[38] Pang, M., Lin, J., Fu, J., Xing, R., Luo, C., and Han, Y., Preparation, patterning and luminescent properties of nanocrystalline Gd_2O_3: A (A= Eu^{3+}, Dy^{3+}, Sm^{3+}, Er^{3+}) phosphor films via Pechini sol–gel soft lithography. *Optical Materials*, 23(3-4):547-558, 2003.

[39] Blasse, G., Energy transfer in oxidic phosphors. *Philips Research Reports*, 24(2):131-&, 1969.

[40] Prabhu, N.S., Somashekarappa, H., Sayyed, M., Alhuthali, A.M., Al-Hadeethi, Y., and Kamath, S.D., 0.25–30 kGy γ Irradiation-induced modifications on the density, optical absorption, thermo-, and photo-luminescence of the 10BaO–20ZnO–20LiF-49.3 $B_2O_{3-0.7}$ Er_2O_3 glass. *Journal of Luminescence*, 231:117820, 2021.

[41] Kaur, S., Pandey, O., Jayasankar, C., and Chopra, N., Effect of gamma irradiation on physical, optical, spectroscopic and structural properties of Er3+-doped vitreous zinc borotellurite. *Journal of Luminescence*, 235:118031, 2021.

[42] Viswanath, C.D. and Jayasankar, C., Photoluminescence, γ-irradiation and X-ray induced luminescence studies of Sm^{3+}-doped oxyfluorosilicate glasses and glass-ceramics. *Ceramics International*, 44(6):6104-6114, 2018.

[43] Zhu, C., Yang, Y., Chen, G., Baccaro, S., Cecilia, A., and Falconieri, M., Photoluminescence and gamma-ray irradiation of $SrAl_2O_4:Eu^{2+}$ and $Y_2O_3:Eu^{3+}$ phosphors. *Journal of Physics and Chemistry of Solids*, 68(9):1721-1724, 2007.

[44] Romanov, N., Malova, M., Lahderanta, E., and Musikhin, S., Effect of gamma radiation on luminescence and photoconductivity of MEH-PPV–lead sulfide nanocomposite, *St. Petersburg Polytechnical State University Journal. Physics and Mathematics,* 11(4):33-43, 2018.

[45] Pandey, A., Sharma R, K., Bahl, S., Kumar, P., and Pal L, S., Radiation dosimetry using nano-$BaSO_4$:Eu. 2015.

[46] Ansari, A., Mohanta, D., and Saha, A., Exploiting valence band mapping and select blue-green and red phosphorescence decay of γ-irradiated nanoscale Eu^{3+}: Gd_2O_3 below concentration quenching. *Optical Materials*, 122:111627, 2021.

[47] S. Horowitz, Y., Satinger, D., and Avila, O., Theory of heavy charged particle thermoluminescence response: the extended track interaction model. *Radiation protection dosimetry*, 100(1-4):91-94, 2002.

[48] Tamilmani, V., Mukhopadhyay, L., Rai, V.K., Sreeram, K.J., and Mishra, A.K., Dual mode luminescence from lanthanum orthovanadate nanoparticles. *Journal of Luminescence*, 217:116761, 2020.

[49] Meltzer, R., Feofilov, S., Tissue, B., and Yuan, H., Dependence of fluorescence lifetimes of $Y2O_3:Eu^{3+}$ nanoparticles on the surrounding medium. *Physical Review B*, 60(20):R14012, 1999.

[50] Schmechel, R., Kennedy, M., Von Seggern, H., Winkler, H., Kolbe, M., Fischer, R., Xaomao, L., Benker, A., Winterer, M., and Hahn, H., Luminescence properties

of nanocrystalline $Y2O_3:Eu^{3+}$ in different host materials. *Journal of Applied Physics*, 89(3):1679-1686, 2001.

[51] Tamilmani, V., Mukhopadhyay, L., Rai, V.K., Sreeram, K.J., and Mishra, A.K., Dual mode luminescence from lanthanum orthovanadate nanoparticles. Journal of Luminescence, 217:116761, 2020.

[52] Huignard, A., Gacoin, T., and Boilot, J.-P., Synthesis and luminescence properties of colloidal YVO_4:Eu phosphors. Chemistry of Materials, 12(4):1090-1094, 2000.

[53] Hsu, C. Energy Transfer in Rare Earth Phosphors. Oklahoma State University, 1975.

[54] Mikhnenko, O.V., Blom, P.W., and Nguyen, T.-Q., Exciton diffusion in organic semiconductors. *Energy & Environmental Science*, 8(7):1867-1888, 2015.

[55] Lunt, R.R., Giebink, N.C., Belak, A.A., Benziger, J.B., and Forrest, S.R., Exciton diffusion lengths of organic semiconductor thin films measured by spectrally resolved photoluminescence quenching. *Journal of Applied Physics*, 105(5):053711, 2009.